

Notes from ISC Data Users

Correct Assignment of Rayleigh Waves to Seismic Events

Petra Buchholz and Siegfried Wendt

Institute for Geophysics and Geology

University of Leipzig

Germany

Excerpt from the
Summary of the Bulletin of the International Seismological Centre:

Buchholz, P. and S. Wendt (2023), Correct Assignment of Rayleigh Waves to Seismic Events, *Summ.*

Bull. Internatl. Seismol. Cent., January – June 2020, 57(I), pp. 28–36,

<https://doi.org/10.31905/XUXL0LWV>.

5

Notes from ISC Data Users

5.1 Correct Assignment of Rayleigh Waves to Seismic Events

Petra Buchholz and Siegfried Wendt

Institute for Geophysics and Geology, University of Leipzig, Germany



Siegfried Wendt and Petra Buchholz

Theoretical travel-time tables can be helpful for phase identification of seismograms. First onsets of P/PKP waves generally have residuals not greater than several seconds. For a correct assignment of the surface wave group to an event, estimating the time difference between the first onsets and the surface waves ($t_{Rmax} - t_{P/PKP}$) is important. Here, t_{Rmax} represents the arrival time of the maximum amplitude inside the Rayleigh wave group (R_{max}) and $t_{P/PKP}$ is the arrival time of the first longitudinal body wave, which may correspond to P, Pdif or PKP phase. Tables with ($t_{Rmax} - t_{P/PKP}$) as a function of epicentral distance were published by *Arkangelskaya* (1959) and *Willmore* (1979). The New Manual of Seismological Observatory Practice (NMSOP, *Bormann*, 2012) contains this table in Data Sheet (DS) 3.1. The time accuracy of these published values ($t_{Rmax} - t_{P/PKP}$) is about one minute.

In this short note we used data from Collm geophysical observatory (CLL) in Germany. The station was established in 1935, providing high-quality seismic data and manually reviewed body and surface wave arrivals (*Wendt and Buchholz*, 2014). Not only waveforms corresponding to tectonic earthquakes are analysed but also those of anthropogenic events. An example of such a case, including a seismogram from CLL showing clear arrival of surface waves despite the event being a nuclear explosion, is presented in Figure 5.1. We have interpreted about 81,000 seismograms of teleseismic earthquakes in an epicentral distance range of 10 - 170 deg (Fig. 5.2) recorded at CLL between 2006 and 2019. This makes a unique homogeneous database that contains about 13,000 events with Rayleigh wave measurements. All

03.09.2017 H=03:30: 1.8 41.33N;129.03E h= 0km mb=6.3 (NEIC) NORTH KOREA

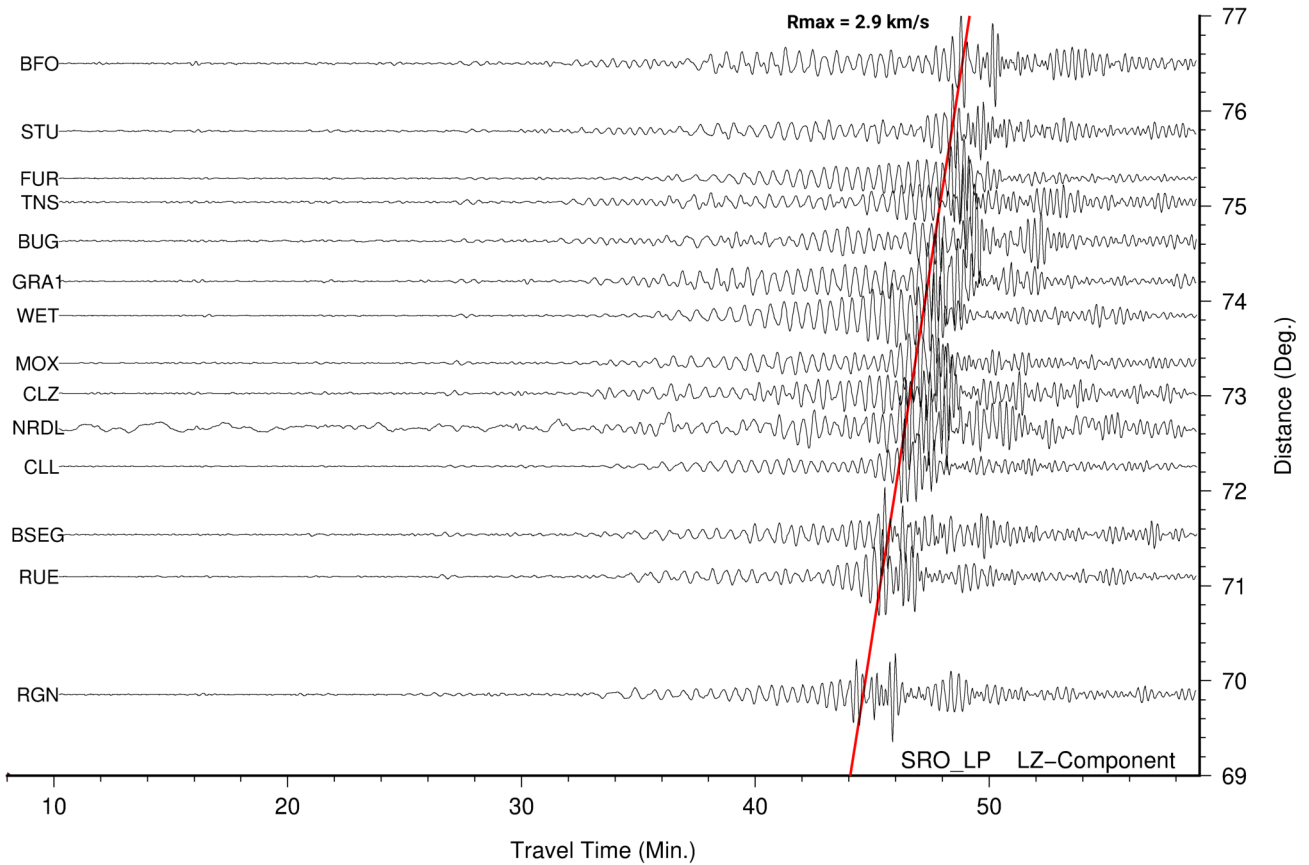


Figure 5.1: Seismograms of an underground explosion in DPRK sorted with respect to distance for stations of the German Regional Seismic Network (GRSN) and GEOFON Network. Horizontal axis shows travel time (in minutes) relative to the origin time of the event (September 3, 2017 03:30:01.8 UTC). The size of event corresponds to $mb=6.3$ or $M_s=5.1$ (NEIC).

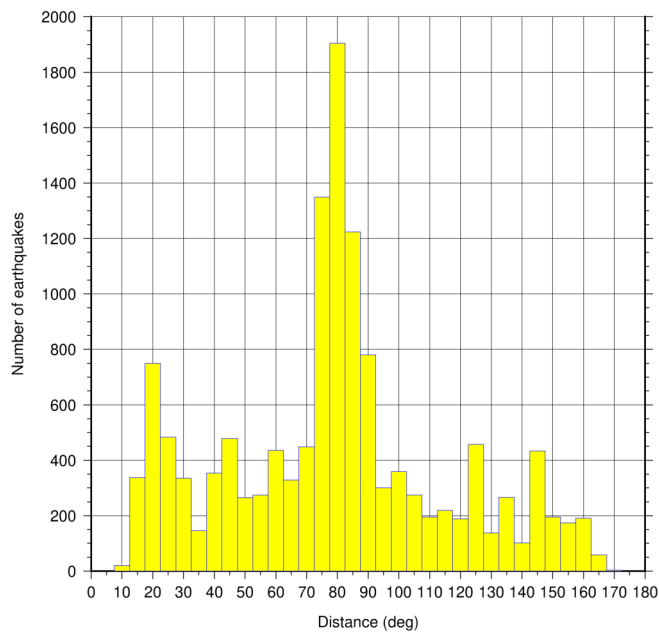


Figure 5.2: Distribution of all events with measured R_{max} on CLL with respect to epicentral distance.

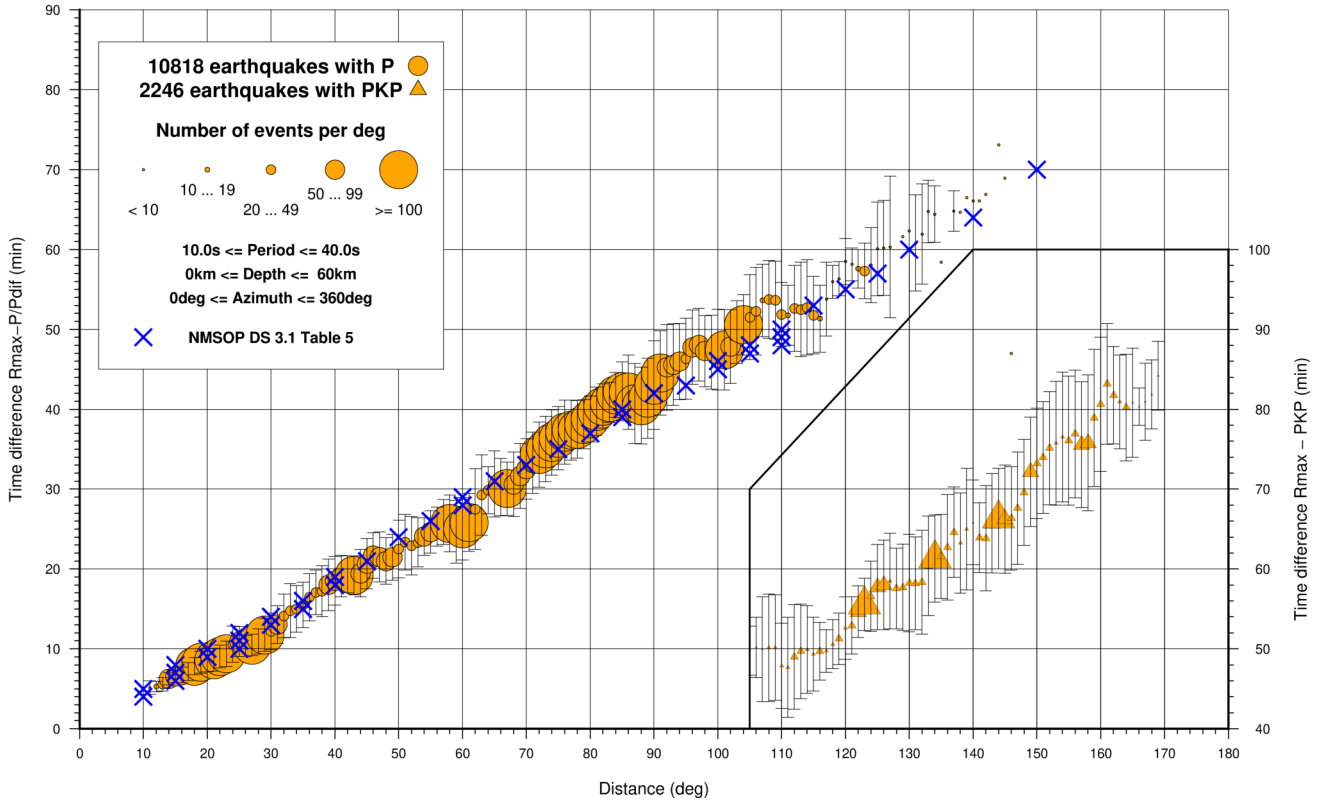


Figure 5.3: Average time differences $t_{Rmax} - t_{P/PKP}$ as function of epicentral distance. Orange circles correspond to $t_{Rmax} - t_P$ values, orange triangles to $t_{Rmax} - t_{PKP}$. Symbol size is proportional to the number of values in the average calculation and thin gray vertical bars represent their standard deviations. Blue crosses represent the values reported in Table 5 of Data Sheet 3.1 from the NMSOP (Bormann, 2012).

Rayleigh waves arrivals were manually picked. Figure 5.3 shows the average time differences between t_{Rmax} and $t_{P/PKP}$ from our dataset as a function of epicentral distance and without differentiating for Rayleigh wave period or ray path (continental or oceanic). There is a general agreement between our values and those reported in the NMSOP (blue crosses). For epicentral distances larger than 105 deg we included Pdif and PKP as the first body wave arrivals and we extended our observations up to 170 deg.

However, the distribution of the average velocities of the Rayleigh wave group calculated for the events recorded at CLL station in grid cells of 2 deg by 5 deg in epicentral distance and azimuth, respectively, highlights significant differences in the group velocities depending on the path (Fig. 5.4). More specifically, predominantly continental paths, such as those within the red sector in Figure 5.4 (epicenters going from the Middle East to the Western Sunda Arc), are characterized by group velocities below 3 km/s. Instead, the blue sector in Figure 5.4 (epicenters including the North Atlantic Ridge and the Caribbean Islands) shows group velocities above 3 km/s for oceanic or mainly oceanic paths (i.e., less than 20% continental path). Some internal, smaller scale variations can also be observed inside the blue coloured sector with the velocities getting smaller due to a larger proportion of continental paths for earthquakes in Iceland or the Mid-Atlantic Ridge.

The histograms shown in Figure 5.5(a) are further highlighting the difference in the Rmax group velocities depending on the path. Indeed, there is a clear shift to values higher than 3.1 km/s and lower than 3.0 km/s for the oceanic and continental paths, respectively. Figure 5.5(b) shows the average group

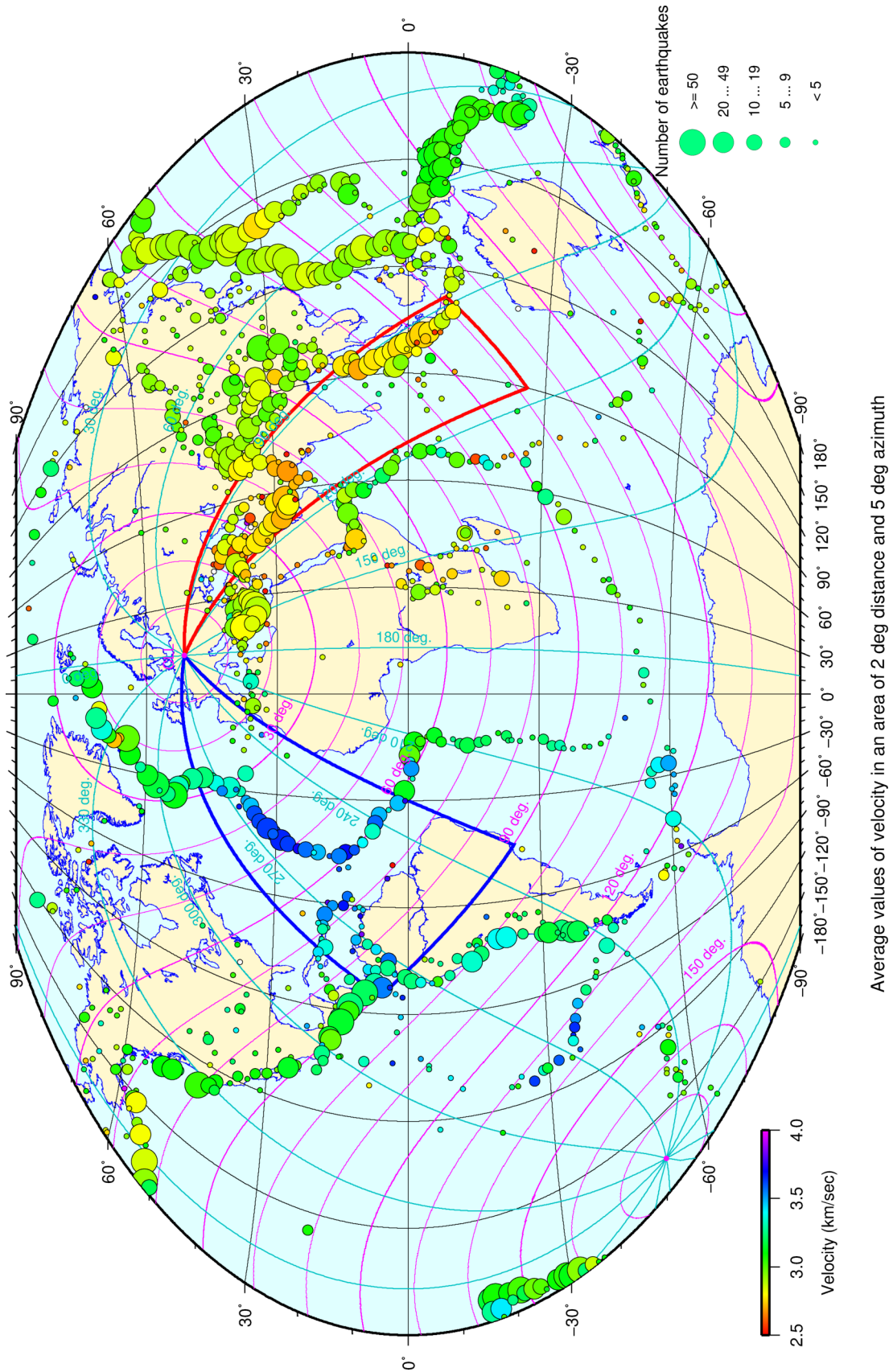


Figure 5.4: Global distribution of maximum Rayleigh wave group (R_{max}) velocity estimated as $(t_{R_{max}} - t_0)/\text{distance}$; with t_0 = origin time of the earthquake. Circles correspond to the averaged individual velocities estimated over 2 deg epicentral distance and 5 deg station azimuth increments for events recorded at station CLL. Size of the circles indicates the number of measurements included in the average calculation. Cyan lines = azimuth, magenta lines = epicentral distance.

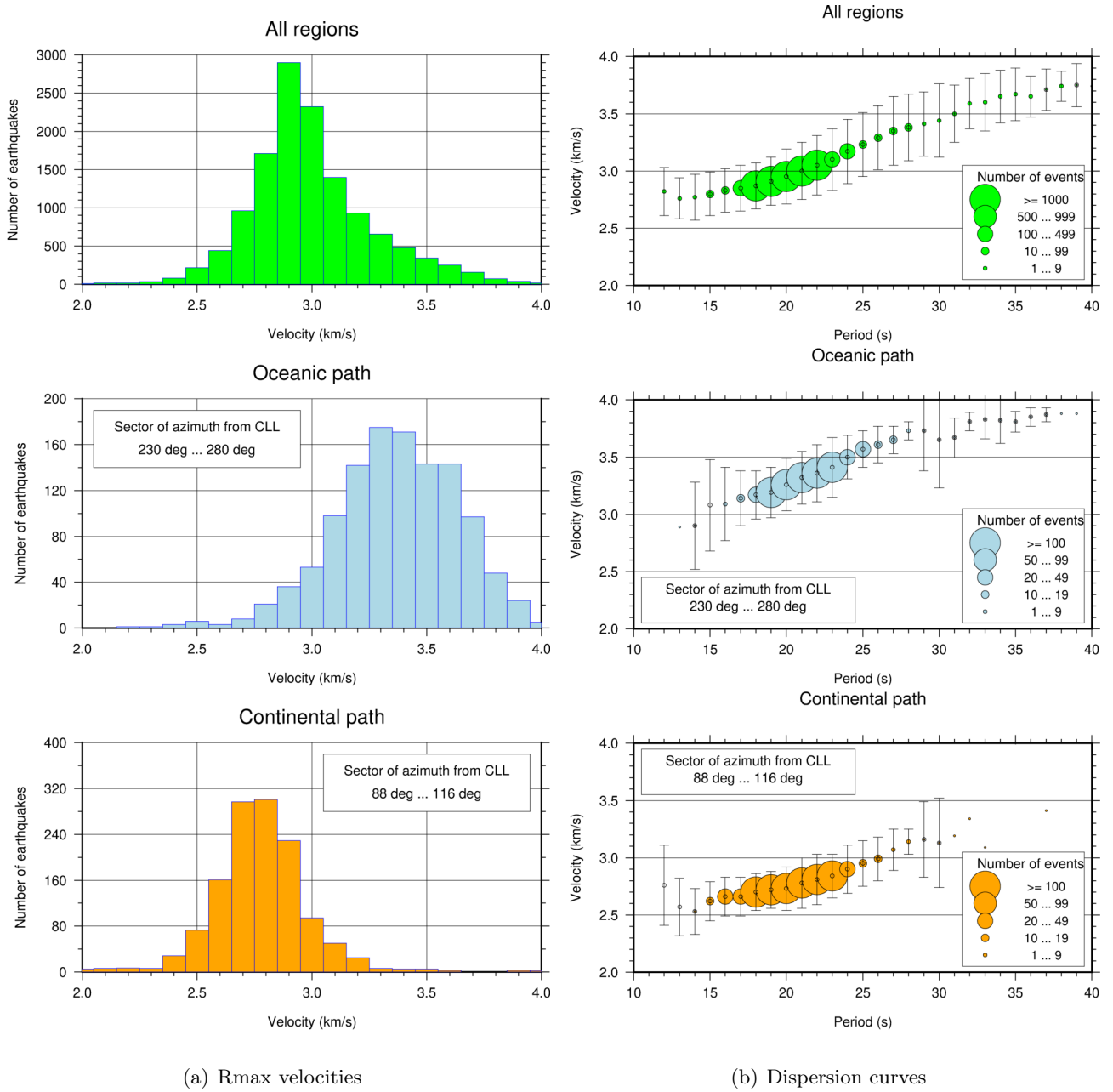


Figure 5.5: Histograms of R_{max} velocities (a) and dispersion curves (b) for: all earthquakes in the database regardless of the region of occurrence (green); sector of 230 – 280 deg azimuth from CLL, corresponding to the predominant oceanic path (blue Fig. 5.4)) and sector of 88 – 116 deg azimuth from CLL, corresponding to the predominant continental path (red in Fig. 5.4).

velocities of R_{max} as a function of the period T for all earthquakes and for the sectors considered in Figure 5.4. We can observe, as expected, that the velocities increase with the period and that the difference between predominantly continental or oceanic paths persists (i.e., higher velocities for oceanic paths and lower for the continental ones).

Considering the results discussed for Figures 5.4 and 5.5, it follows that the dependence of R_{max} velocity on its path should be taken into consideration when estimating the theoretical travel-times $t_{R_{max}}$. With the velocities for period T for continental path and oceanic path defined as $v_{cont}(T)$ and $v_{oce}(T)$, respectively, the theoretical $t_{R_{max}}$ for the overall path D , decomposed in a continental part D_{cont} and

an oceanic part D_{oce} , can be estimated as follows:

$$t_{Rmax} = \frac{D_{cont}}{v_{cont}(T)} + \frac{D_{oce}}{v_{oce}(T)}.$$

We calculate the continental (D_{cont}) and oceanic (D_{oce}) parts of the path D as the intersections of the horizontal component of the ray-path with the coastal lines using the Generic Mapping Tool (command “spatial”; *Wessel et al.*, 2019). Our measurements indicate that such an approach, although it should be considered as a simple and quick approximation, works well when calculating t_{Rmax} for different paths to CLL. However, other more precise approaches can be used. The proposed expression for the travel-time calculation considers the dependence of the Rayleigh wave on period and path and, as such, it is an improvement compared to the travel times estimations by *Archangelskaya* (1959) and provided in Table 5 of DS 3.1 from the NMSOP (*Bormann*, 2012).

Additional challenges in t_{Rmax} estimations may appear due to the complexity of the recorded waveforms. E.g., the superposition of surface waves from two different earthquakes can make the association of the Rayleigh wave measurements to the correct event difficult or impossible by using just time differences. In such instances, sorting the seismograms with respect to epicentral distance can be helpful, especially if there is a distinct difference in the event-station azimuth for the overlapping earthquakes. Figure 5.6

14.03.2010 H=20:33:13.7 2.75S; 83.70E h= 28km Ms=5.5 (NEIC) SOUTH INDIAN OCEAN

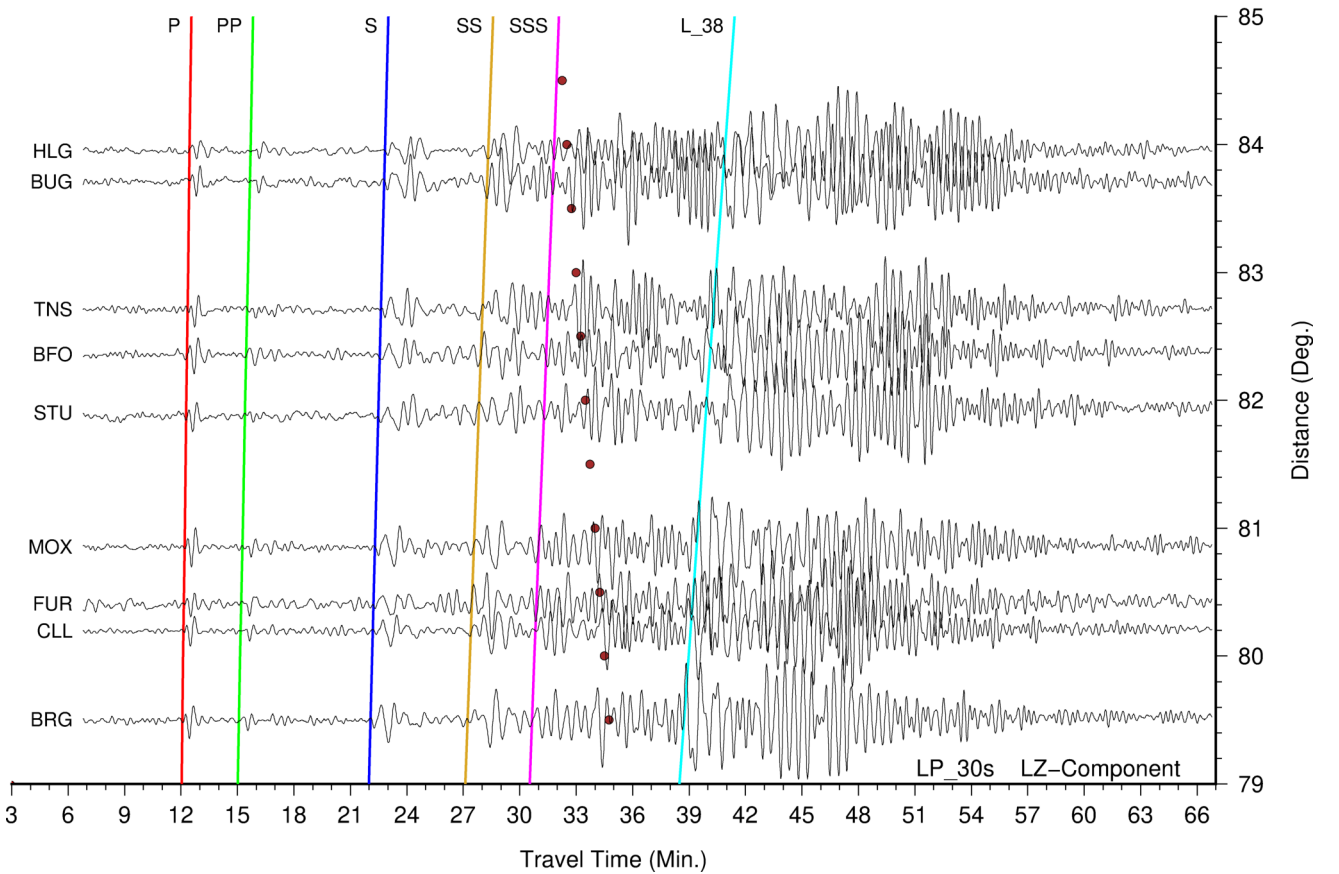


Figure 5.6: Superposition of seismograms of two events: South Indian Ocean (2010-03-14 20:33:11.5) $M_s=5.5$ and Central Chile (2010-03-14 20:04:55.5) $M_s=5.4$ (origin times from ISC) on stations of GRSN and GEOFON networks. cyan line = Rayleigh waves of South Indian Ocean event; brown circles = t_{Rmax} of Chile event. See text for more details.

shows a superposition of seismograms for two events: one from South Indian Ocean ($M_S=5.5$, epicentral distance to CLL = 80 deg) and the other from Central Chile ($M_S=5.4$, epicentral distance to CLL = 117 deg) occurring about 28 minutes before the South Indian Ocean earthquake. These two events have a difference of 134 degrees in back azimuth to CLL. Seismograms of the South Indian Ocean event are sorted with respect to the epicentral distances for stations belonging to the German Regional Seismic Network (*GRSN*) and *GEOFON* Network. Long, periodic initial part of Rayleigh waves is marked by a cyan line with a slope of 3.8 km/s. Body waves (SS, SSS) of this earthquake are superposed by surface waves of the Central Chile earthquake. Its t_{Rmax} timings are marked by brown circles. The surface waves of the two events can be distinguished by their arrivals on the stations sloping in different directions (cyan line and brown circles). Without sorting seismograms by epicentral distance, the identification and correct association of the surface wave for the Central Chile earthquake may not be possible or it may contain erroneous measurements.

It is also worth mentioning that surface waves can travel around the Earth several times and be observed as returning waves after large earthquakes. This can occur on the short path from the hypocenter to seismic station ($360 \text{ deg} + D$) as well as on the long path ($360 \text{ deg} + (360 \text{ deg} - D)$), where D is the epicentral distance in degrees. Such waves can add complexity to the seismic recordings and hinder the association of surface waves to the correct event. Figure 5.7 shows an example where seismograms of GRSN stations are sorted with respect to the epicentral distance. Surface wave trains L, L3 and L5

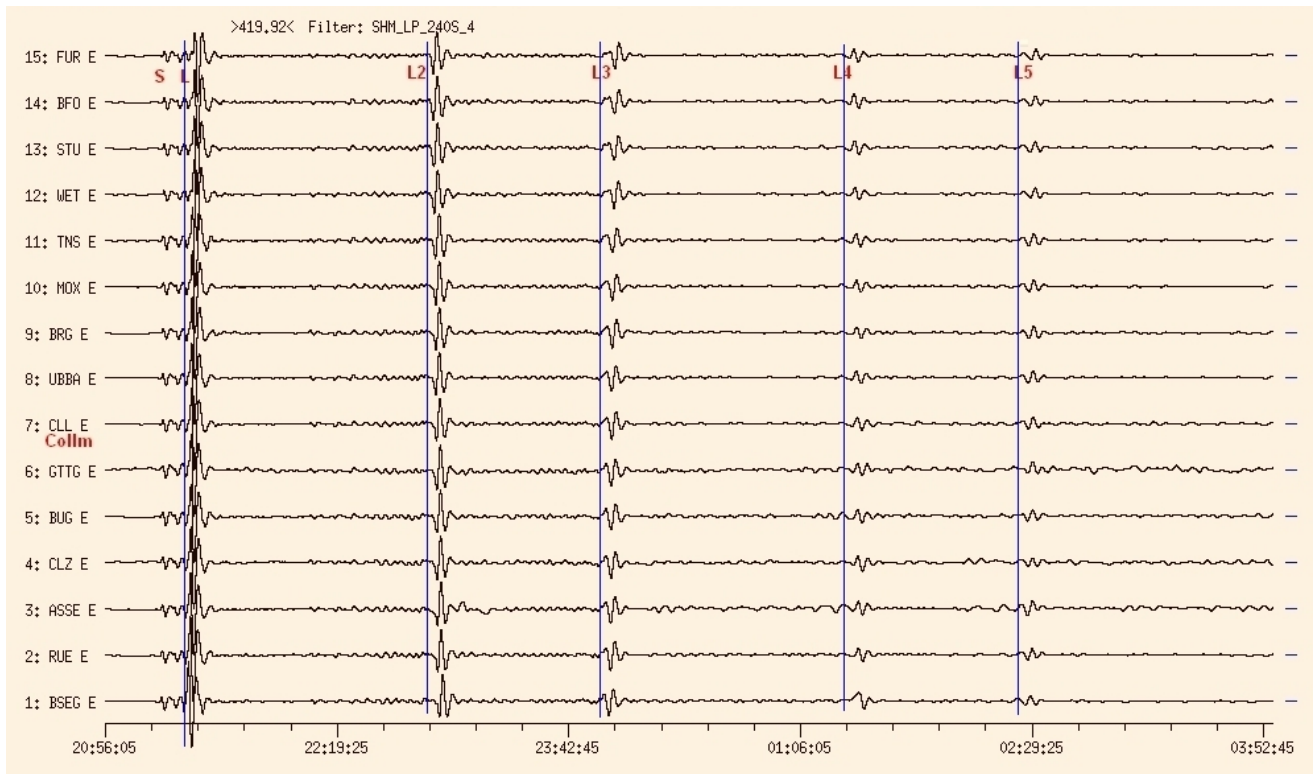


Figure 5.7: Seismograms showing surface waves of a strong earthquake ($m_b=7.0$, $M_S=7.6$, ISC) south of Alaska on October 19, 2020, 20:54:39.0 GMT. The surface waves travelled up to two times around the globe along the short and long path from the earthquake to CLL. L, L3 and L5 – travelled along (multiples of) the short path, L2 and L4 – along (multiples of) the long path. Blue line = arrival time at CLL. Please note that $L(m/V)$ is an older notation for the maximum of the surface wave and does not refer to Love waves specifically here.

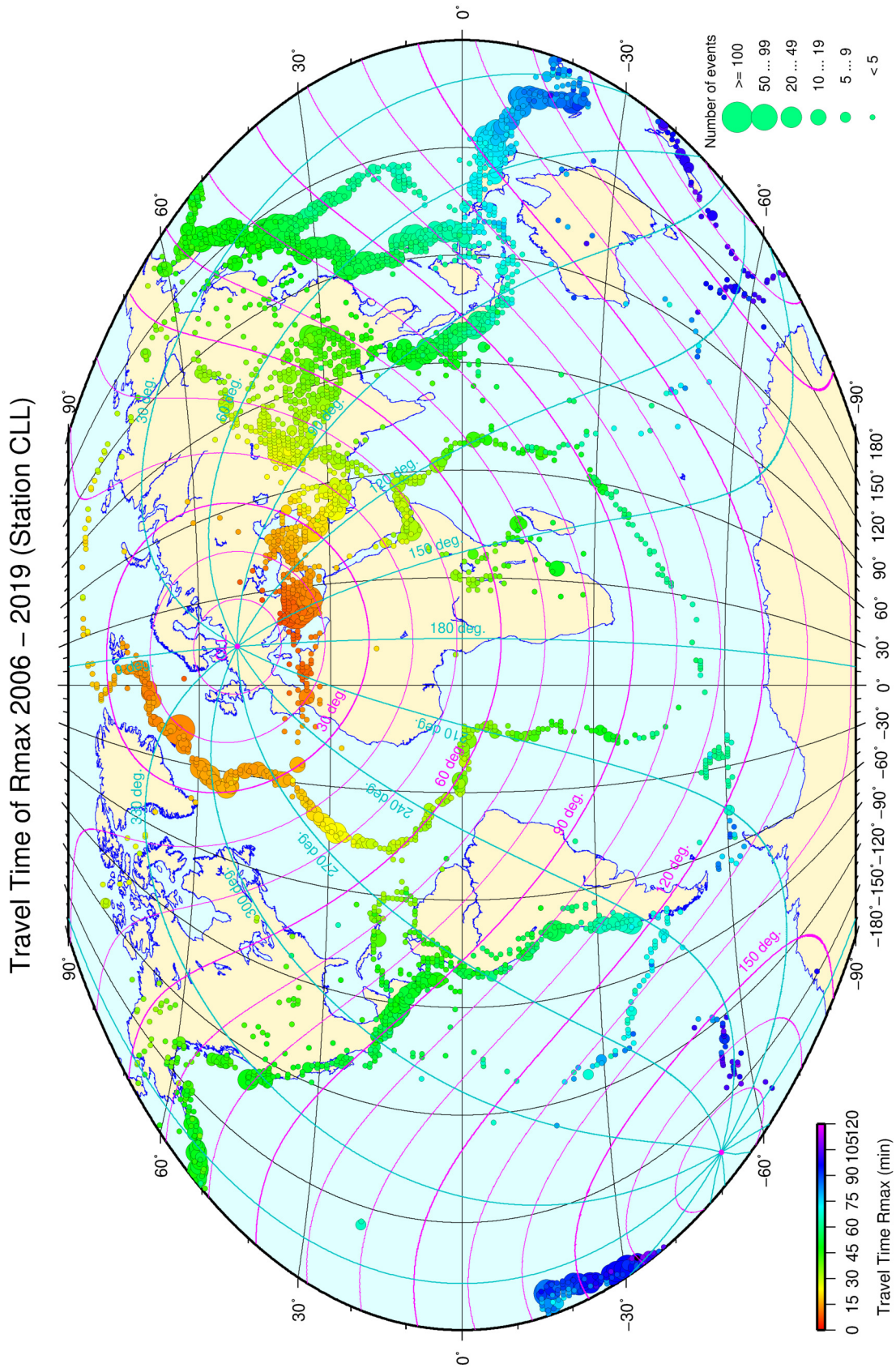


Figure 5.8: Overview of global Rmax travel times ($t_{Rmax} - t_{P/PKP}$) recorded in CLL. Circles = number of events in cell, cyan lines = azimuth, magenta lines = epicentral distance.

correspond to the travel-paths along the short path while L2 and L4 to the travel-paths along the long path ($L2 = 360 \text{ deg} - D$, $L3 = 360 \text{ deg} + D$, $L4 = 360 \text{ deg} + (360 \text{ deg} - D)$, $L5 = (2 * 360 \text{ deg}) + D$, i.e. L5 travelled around the Earth twice before arriving at CLL station). The path of the wave-train can be identified from the seismograms: L, L3 and L5 arrive first at the closest station (BSEG) in Northern Germany, while L2 and L4 arrive first at the furthest station FUR in Southern Germany.

In this short note we presented our database of teleseismic Rayleigh wave travel-time observations (t_{Rmax}) at station CLL in Germany and provided a procedure to better estimate the expected arrival times of t_{Rmax} by separating the wave propagation path into the continental and oceanic sections. The database provided can serve for the observation-based Rayleigh wave travel-time estimations at CLL station for future earthquakes. The summary of the global Rayleigh wave travel-times included in the database is provided in Figure 5.7. The dataset containing all the associated picks used in this study is publicly available in the ISC Dataset Repository (Wendt and Buchholz, 2023). By creating a 1 deg by 1 deg grid of this map, we can estimate a time window when Rmax should arrive at the station when analysing the seismograms. This map is of course only based on the measurements at CLL station, but with a large enough dataset, this principle could be used by other observatories and institutions, which would lead to more accurate estimations of the Rayleigh wave arrivals on a global scale.

Acknowledgements

The authors are very grateful to Natalia Poiata and Kathrin Lieser from the International Seismological Centre (ISC) for their constructive suggestions, which helped improve this contribution.

The authors thank Prof. Dr. Michael Korn for a critical reading of the manuscript and useful hints.

References

- Arkangelskaya, V .M. (1959), The dispersion of surface waves in the Earth's crust, *Izv. Akad. Nauk SSSR, Seriya Geofiz.*, 9 (in Russian).
- Bormann, P. (Ed.)(2012), New Manual of Seismological Observatory Practice (NMSOP-2), *Potsdam : Deutsches GeoForschungszentrum GFZ; IASPEI*, <https://doi.org/10.2312/GFZ.NMSOP-2>.
- GEOFON Data Centre (1993), GEOFON Seismic Network, GFZ Data Services, GFZ German Research Centre for Geosciences, Potsdam, Germany, <https://doi.org/10.14470/TR560404>.
- GRSN, Federal Institute for Geosciences and Natural Resources (1976), German Regional Seismic Network (GRSN), Bundesanstalt für Geowissenschaften und Rohstoffe (BGR), Hanover, Germany, <https://doi.org/10.25928/mbx6-hr74>.
- Willmore, P. L. (Ed.)(1979), Manual of Seismological Observatory Practice, *World Data Center A for Solid Earth Geophysics, Report SE-20*, Boulder, Colorado.
- Wendt, S. and P. Buchholz (2017), Collm Geophysical Observatory, *Summ. Bull. Internatl. Seismol. Cent.*, January - June 2014, 51(I), pp. 32–44, <https://doi.org/10.5281/zenodo.996043>.
- Wendt, S. and P. Buchholz (2023), Rayleigh wave travel times measured at Collm Geophysical Observatory, Germany, between 2006 and 2019, ISC Seismological Dataset Repository, <https://doi.org/10.31905/PHF064PS>.
- Wessel, P., J. F. Luis, L. Uieda, R. Scharroo, F. Wobbe, W. H. F. Smith and D. Tian (2019), The Generic Mapping Tools version 6, *Geochem. Geophys. Geosyst.*, 20, 5556–5564, <https://doi.org/10.1029/2019GC008515>.